Journal of Engineering Science and Technology
Vol. 13, No. 4 (2018) 977 - 989

EFFECT OF GROUNDWATER SALINITY LEVEL ON SOIL USING REMOTE SENSING AND GIS TECHNIQUES: CASE STUDY OF SOUTHWEST OF BASRA PROVINCE

MUSHTAK T. JABBAR[1], AMMAR S. DAWOOD[2,*], HAYFAA J. AL-TAMEEMI[3]

[1]Geology /Earth Sciences/ HCC/ Seattle, Washington, 98198 USA,
[2]Department of Civil Engineering, University of Basrah, Iraq
[3]Department of Soil Science and Water Resources, Universityof Basrah, Iraq
*Corresponding Author: ammars.dawood@yahoo.com

Abstract

Groundwater salinity level is one of the most important considerations for monitoring soil degradation that threat some regions in the southwest of Basra Province, Iraq. The aim of this research is to assign the appropriate and effective image processing techniques to be implemented for monitoring, and then to evaluate groundwater salinity level map. Landsat TM 2000 and ETM 2015 images respectively have been selected, as well as ancillary data of the available salinity field measurements have been used. Spatial overlay analysis between salt affected areas and water table were made to assess spatial distribution as well as relationships with these features. The result shows that about 47.8% of the areas were low-saline in 2000. This gradually decreased to 35.9% in 2015. Large area change was observed in the slightly and moderately saline soil categories. High sensitive areas of saline soil were about 13.3% in 2000 and this increased to 19.4% in 2015. Areas highly vulnerable to salinization were related to the groundwater salinity level that normally occurred on the soil sediment in this location of study.

Keywords: Groundwater salinity level, Salinity Index, remote sensing, GIS, Iraq.

1. Introduction

Groundwater salinity level is one of the main problems of soil degradation; it is an environmental hazard that causes losing the agricultural productivity. Surface salinity processes are highly dynamic, so using multi-date images are a suitable way to detect the changing state of soil, as well as the technology development and extent of environmental change over the last 20th century has given a new

Nomenclatures

E	Longitude, degree
N	Latitude, degree
pH	Potential of hydrogen
TH	Total hardness, mg/L
TDS	Total dissolved solids, mg/L
SO_4	Sulfate or sulphate, mg/L
Na	Sodium, mg/L
Ca	Calcium, mg/L
NO_3	Nitrate, mg/L

Abbreviations

ETM	Enhanced Thematic Mapper
FAO	Food and Agriculture Organization
GIS	Geographic Information System
MLC	Maximum Likelihood Classifier
RS	Remote Sensing
SI	Salinity Index
TM	Thematic Mapper
WRS	Worldwide Reference System

urgency for monitoring this change. Wide ranges of processing techniques are available to discriminate the spectral response in regard to the different soil quality [1-3].

There are numerous studies on groundwater-associated salinity, but more information is required on the effects of groundwater dynamics on soil salinization. Frequent irrigation with small quantities of water is effective to reduce soil surface salt accumulation induced by saline shallow groundwater. Salt excess in soils has detrimental effect on crop yields and agricultural production due to poor land and water management, and results in substantial losses of arable soils, especially in the arid and semi-arid areas [4]. Furthermore, salinity also affects other major soil degradation phenomena such as soil dispersion, increased soil erosion, and engineering problems [5].

However, soil salinity is quite time and space dynamic as salinization is the consequence of different complex processes of salt redistribution that depends on natural conditions, system features, agricultural practices and drainage management. In addition, observing the returns and benefits of drainage takes a long time (often more than 25 years) that instantaneous measurements of salinity do not reflect current conditions [6]. Observations of many irrigated areas in the world also shows that water logging and salinization typically appear only 10-50 years after the beginning of the project, depending on the initial depth and recharge rate of the water table and on drainage conditions.

Large scale and multi temporal studies of salinity, especially long term changes in salinity help to understand the nature of salinization and to evaluate the effectiveness of salinity control practices. Remote sensing and GIS techniques have become tools for the purpose of identifying and classifying saline soils [3, 7]. This technique is efficient, cost effective, fast, labor saving and accurate for

delineating salt affected soils. The integration of remote sensing data, in the form of satellite imagery, with GIS has boosted up the ability of delineating and mapping soil salinity. Several studies have proved that remote sensing is a promising method to identify salt affected soils, especially those with moderate and high salinity levels [8, 9].

2. Materials and Methods

2.1. Study area

The study area located in the southern parts of Iraq, lies within longitude 47° 43′ to 47° 45′ E and from latitude 30° 18′ to 30° 21′ N with the total area: 17.792 sq.km (Fig. 1). The soil of Iraq is considered as sedimentary soil, especially in the central and southern parts. The annual humidity is less than 50% and remains less than 30% during the daytime. The average evaporation exceeds 2450 mm/year with average annual rainfall less than 100 mm.

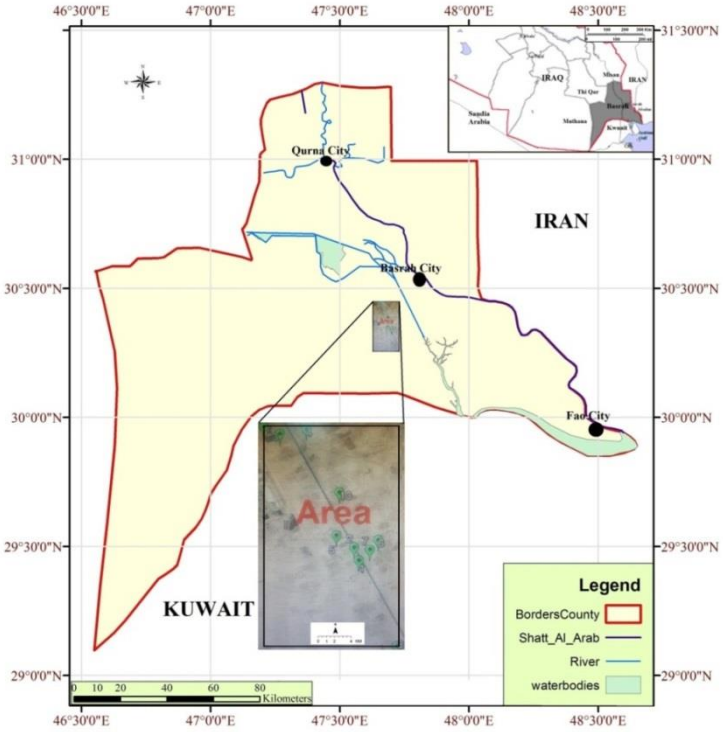

Fig. 1. Location of study area in the southern part of Iraq.

2.2. Methods

This research used different analyses, which involves remote sensing for salinity change detection, GIS assisted spatial modeling, regression analysis and finally validation and comparison of the methods. It involves the integration of thematic layers such as geological information, elevation, groundwater salinity level (Table 1), soil texture and vegetation density in mapping soil salinity.

Table 1. Some physical and chemical properties of groundwater.

Well No.	E	N	EC	TDS	Cl	SO_4	Na	Mg	Ca	NO_3
1	47.74401	30.31809	11300	8528	2850	2000	2510	230	592	51.19
2	47.74331	30.32003	7900	6000	1805	1500	1550	163	544	41.29
3	47.73203	30.33773	7580	5926	1710	1100	1500	528	800	22.2
4	47.73604	30.33841	15750	13000	4750	1500	4500	579	1280	51.49
5	47.74075	30.32178	8510	6688	1353	1400	1700	235	562	53.79
6	47.74677	30.32113	9210	7226	2233	1500	2130	221	608	29.3
7	47.74558	30.31972	8770	5948	1552	1800	1400	197	530	16.63
8	47.74912	30.30631	7190	5902	1455	1600	1200	207	562	13.48
9	47.72943	30.33897	7940	5610	1710	1150	1500	207	546	51.08
10	47.74113	30.32837	9420	6628	2090	1450	1800	160	499	29.95

Landsat images of TM 2000 and ETM 2015 were acquired for the study area (Table 2). Layer staking was made for all six bands excluding the thermal band. Geometric correction for the three Landsat images was accomplished using a topographic map of the study area [9]. Landsat images were registered to the topographic map using control points, which were easily recognizable on the satellite image. Image enhancement was made to improve the interpretability of the images.

Table 2. Remote sensing data that used in the study.

Location	Satellite Sensor	*WRS Path/Row	Date
Al Basra- Al-Zubair	**Landsat-5 TM**	**166/40**	**July 10, 2000**
	Landsat-7 ETM	**166/40**	**July 18, 2015**

* WRS is the Worldwide Reference System (WRS), which is a global notation system for Landsat data.

In this research, a maximum likelihood classifier (MLC) was used to retrieve urban cover areas water bodies, bare land, vegetation density, and sand land area. Because the assemblages are mixed in the class to be mapped, they will generally be referred to as land use/cover class. Supervised methods proved superior and are covered below. Density maps were created by correlating several test land use/cover detection to ground data from published classification map about the location area. Urbanization properties, water bodies, bare land, vegetation density, and sand land area can be delineated on an image to gather the spectral response for similar areas in the rest of the image. By gaining a prior knowledge of an area on the image to be classified, response across all bands was matched using supervised methods to produce desirable output classes. Salt affected areas were clearly identified from other features by higher reflectance in many bands. However, it was difficult to differentiate salt affected area from sand soils. Salinity Index (S.I.) proposed by Tripathi et al. [10] was applied, which gives relatively good results in the re-classification of salt-affected soils. The S.I is calculated as

$$S.I = (Band1 \times Band3)^{1/2} \quad (1)$$

where, band1 and band3 represent the spectral bands of the Landsat images.

Therefore, sample sites identified as salt affected were used for image analysis, followed by site verification. Topographic maps of 1:50,000, were used in digitizing thematic layers for the overlay analysis. A soil map of 1:10,000 and

geology map of 1:250,000 of the area were obtained from FAO soil classification and Geological Survey of Basra Province, respectively. To assess the spatial distribution of salt affected area with respect to groundwater table. For the purpose of interpolation, 10 wells and soil sample data were selected and interpolated to generate a continuous surface distributed throughout the study area were used. A total of 10-point data with coordinate references were acquired and converted in to point shape file in GIS environment. For the spatial overlay analysis, the groundwater table point data were interpolated to generate continuous surface water table using spatial analysis tools in GIS environment. During interpolation, the raster data were sampled to 28.5 sq.m cell size to be made compatible with other layers in the analysis [11, 12]. After interpolation, the continuous surface water table data were reclassified into three classes based on its contribution to the salinization process [1, 4, 13]. According to the soil salinity data, extents of soil salinization were graded as series of > 5% (I), 2%-5% (II), 0.5-2% (III), < 0.5% (IV), which denote high salinization, medium salinization, low salinization, unaffected, respectively (Table 3) [11-13]. All the thematic layers were generated in GIS environment at a scale of 1:250,000. The software's packages used for this study were (ERDAS ver. 9.1) and GIS (ArcGIS ver. 9.2).

Table 3. Land surface features of pure pixels.

Surface features	Biomass (kg/30 m^2)	Soil moisture (%)	Soil salinity (%)	Salinity grades
Sand area	0.09	0.1	0.05	IV
Sparse vegetation area	14.5	8.9	1.96	III
Luxuriant vegetation area	26.6	18.5	0.42	IV
Wet salty crust	1.3	21.9	9.18	I
Dry puffy salty crust	2.2	4.6	7.94	I
Salty meadow	4.9	5.8	3.67	II

Many models and indicators exist that are used to analyse the magnitude, rate and trend of land degradation risk [14-16]. In order to quantify land use/cover changes and their regional disparity, Land Degradation Risk (LDR) was calculated using the following equation [17]:

$$LDR = \sum_{ij}^{n} S_{i\text{-}j} \Big/ \sum_{i=1}^{n} S_i \times (t_2 - t_1)^{-1} \times 100\% \quad (2)$$

where LDR_k stands for annual detection of land degradation for study area from time t_1 to t_2, S_i is the area of land use/cover type at time t_1, $S_{i\text{-}j}$ is the change in area for a land parcel whose cover type changed from i to j between t_1 and t_2 (I,j= 1,2,3,4 i≠j); n represents the total number of land use/cover types which is four. Able to show dynamics of land use/cover changes and their variation across different regions [18].

The land use/cover change map derived from the satellite image was digitized and edited in ArcGIS. Other derived attribute data, viz., and population pressure, were incorporated into the GIS database using FoxPro®. Final tally of land use/cover change for study area was determined by merging all ranks of change associated with the land use/cover indicators. Prior to the merging, each rank level was converted into a numerical value according to an established linear and continuous mathematical equation. The area of land use/cover detection at each

overall level of change within study area was ascertained by overlaying the final land use/cover change map with the administrative boundary map using ArcGIS.

3. Results and Discussion

Table 4 shows significant changes in the LULC can be recognized and type of LULC conversion taking place can be identified. From 2000 to 2015 sand land, urban areas, and bare lands saw a relatively dramatic increase. The areas that contributed the most to this change were vegetation land. This may suggest logging and development. During the same time span, urban areas also increased in size. The majority of this change came from the development of vegetation land into an urban class. Water bodies saw a decrease 10.6% in size. Some of the water bodies converted to unused land, while some of it was converted to urban. Vegetation areas also saw a decrease in size. Most of it was converted to sand cover area, while a smaller but significant portion was developed into urban areas.

Table 4. (LULC) classes monitored from satellite image for the study area.

(LULC) classes	Area 2000		Area 2015		Amount Change	
Vegetation land	**km^2**	**%**	**km^2**	**%**	**km^2**	**%**
Sand land	5.32	29.9	4.68	26.3	-0.64	-12.0
Urban area	5.64	31.7	6.03	33.9	0.39	6.9
Unused land	1.83	10.3	2.12	11.9	0.29	15.8
Water bodies	2.75	15.5	2.95	16.6	0.20	7.2
Vegetation land	2.25	12.6	2.01	11.3	-0.24	-10.6

Two scenes for each of Landsat TM and ETM+ for the period 2000 and 2015 respectively have been used to create an image index of Salinity Index (SI) depending on the spectral response of the soil. This index reveals an increase in salt-affected area during the mentioned period. Ancillary data is accurate strategy that indicators different salinity level in the term of spectral response. The results show the incorporation of the EC relationship with Na^+, Ca^{++}, and Mg^+ content which provides a better and more objective indicator of soil salinity and indicates that there is greater soil salinity with increasing Cl, SO_4, and NO_3 content. Accordingly, many information layers of the salinity elements have been created as shown in Figs. 2 and 3. As well as there is good contribution between EC and spectral response in Landsat images specifically in Band 1 and Band 3 which is considered the most accurate band to detect and evaluate soil salinity.

The salinity index (SI) was used to enhance the saline zones and suppressing the vegetation, which was calculated as the ratio of the difference of red band to NIR band. The values of the salinity index (SI) ranged between 1 and –1, from these areas with value 0 and less than 0 were classified as none saline. About 47.8% of the study area was low sensitive areas in 2000, which gradually decreased to 35.9% in 2015 (Table 5). Out of this, 8.50 km^2 under low sensitive areas in 2000, whereas the rest area was changed in to slightly saline. Moderately saline soil was about 38.9% in 2000, which was increased to 44.7% in 2015, respectively.

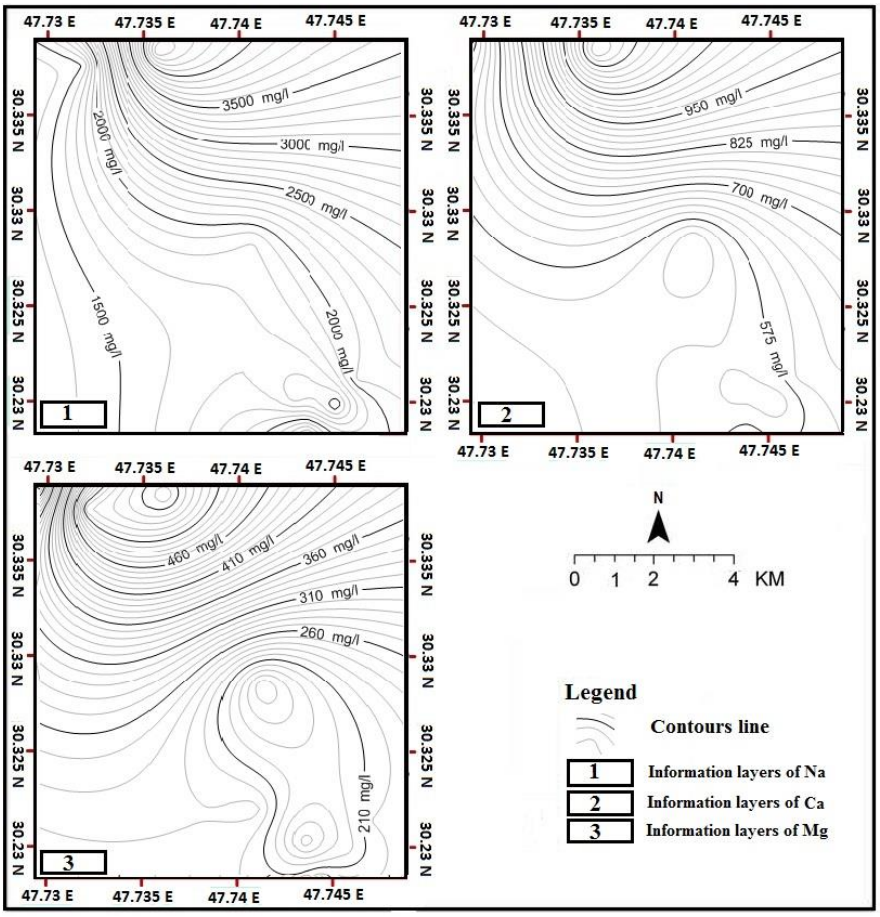

Fig. 2. Information layers of Na, Ca, and Mg as contours line.

Table 5. Salt affected area class derived from SI and change rate for 2000 and 2015.

Salt affected area class	Area 2000		Area 2015		Rate of Change	
	km^2	%	km^2	%	km^2	%
Low sensitive areas	8.50	47.8	6.39	35.9	-2.11	-11.9
Moderately sensitive areas	6.92	38.9	7.95	44.7	5.80	32.6
High sensitive areas	2.37	13.3	3.45	19.4	6.10	34.3
Total	17.792	100	17.792	100	-	-

The results indicate that salt affected areas were distributed throughout the study area. In the central and in many of the northern parts of the farm was moderately saline. As illustrated in Fig. 4, the north-western parts of the location were of high salinity. A map of salt affected soil for the two different study years revealed that moderately and slightly saline soils were concentrated in the central area of the study location. Figure 4 shows the area ratios and statistics characteristics of soil salinity of different groundwater depth types in the study area. There are clear

differences of soil salinity among them. As soil salinity problem was closely related with salt water concentration, the salt affected areas mapped were overlaid with the groundwater table depth. The Groundwater table depth of the area was within 10-30 m below the ground surface. About 54% of the salt affected area of groundwater salinity level. The classification of groundwater table depth with different level class and risk salt water concentration indicated that groundwater salt content is the major problem of the occurrences of soil salinity especially in critical areas. From the prediction model, the total area identified as salt affected soil was 25%. Out of this, 11% is lying within critical areas and 64% was lying in potentially area classes of the total salt affected soil exists (Fig . 4).

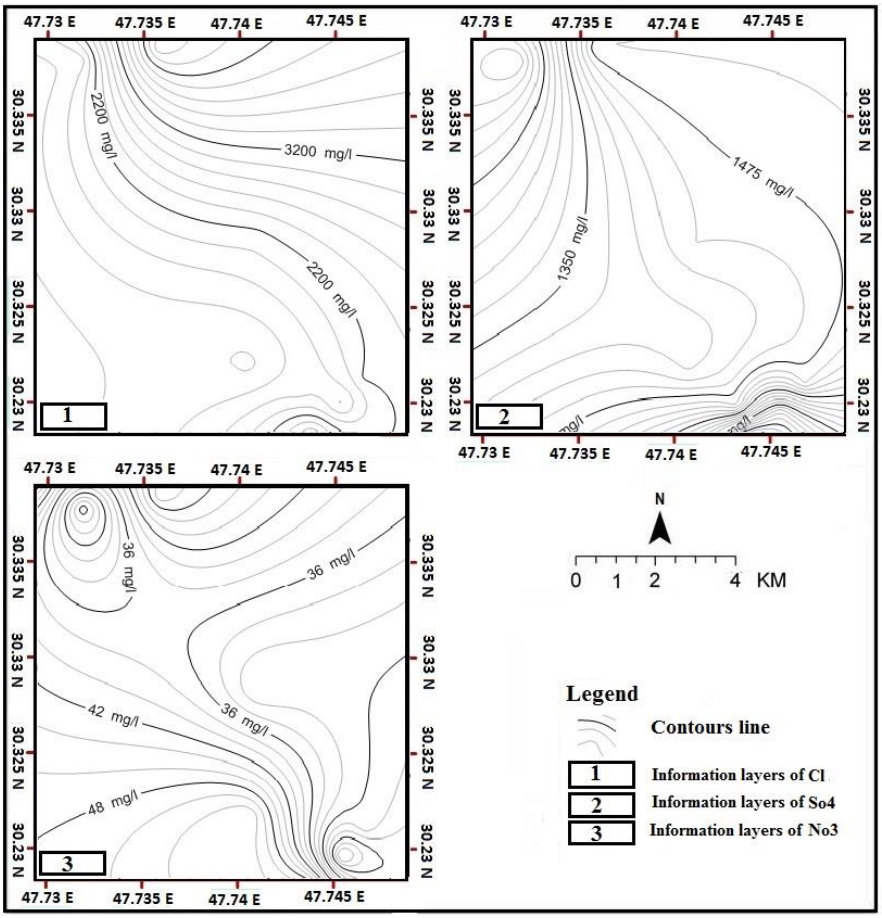

Fig. 3. Information layers of Cl, SO_4, and NO_3 as contours line.

Since salinity is a dynamic process it is important to monitor salinity process and map its spatial distribution regularly. Although geostatistical technique is available to see the spatial structure it takes lots of effort in collecting sufficient soil samples and their laboratory analysis (Fig. 5). In this respect combination of geopedologic interpretation of the area and incorporation of band rotation seems to be useful in accessing salinity problem quickly. Results, using spatial analysis methods, showed that 11.2% of land had no risk of land degradation by soil

salinity, 26.1% had moderate, and 62.7% of the total land area was at a high risk of land degradation by soil salinity. In conclusion, the study area is exposed to a high risk of soil salinity. The results of the statistical analysis showed that saline area has a significant correlation with vegetation cover negative change (0.89).

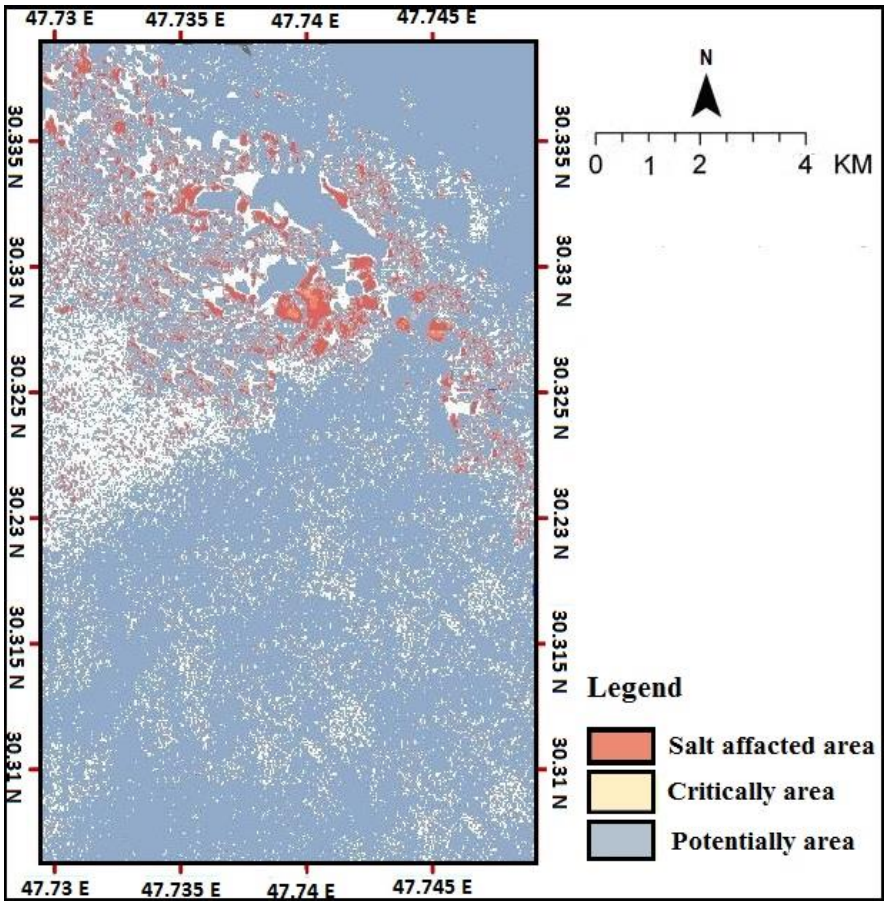

Fig. 4. Created salinity index (SI) for the periods 2000 and 2015.

The area of salt affected soils that resides within 100 m and 300 m distance of wells are found to be only 40.8% and 29.3%, respectively (Fig. 5). The result indicated that poor irrigation and water management systems and small canal structures lead to secondary salinization. Secondary salinity resulting from modern irrigation occurs due to accelerated redistribution of salt in the profile by high water table. Irrigation was the main cause of rise in shallow groundwater table under intense evapo-transpiration conditions and this led indirectly to soil salinization. In general, stretching from the wells buffer, soil salinity shows decreasing tendency with the decrease in distance from the wells buffer. It reflects the significant influence on soil salinity by the salt water around. . The statistical analysis showed this index (SI) has a significant correlation with water bodies' positive change (0.92).

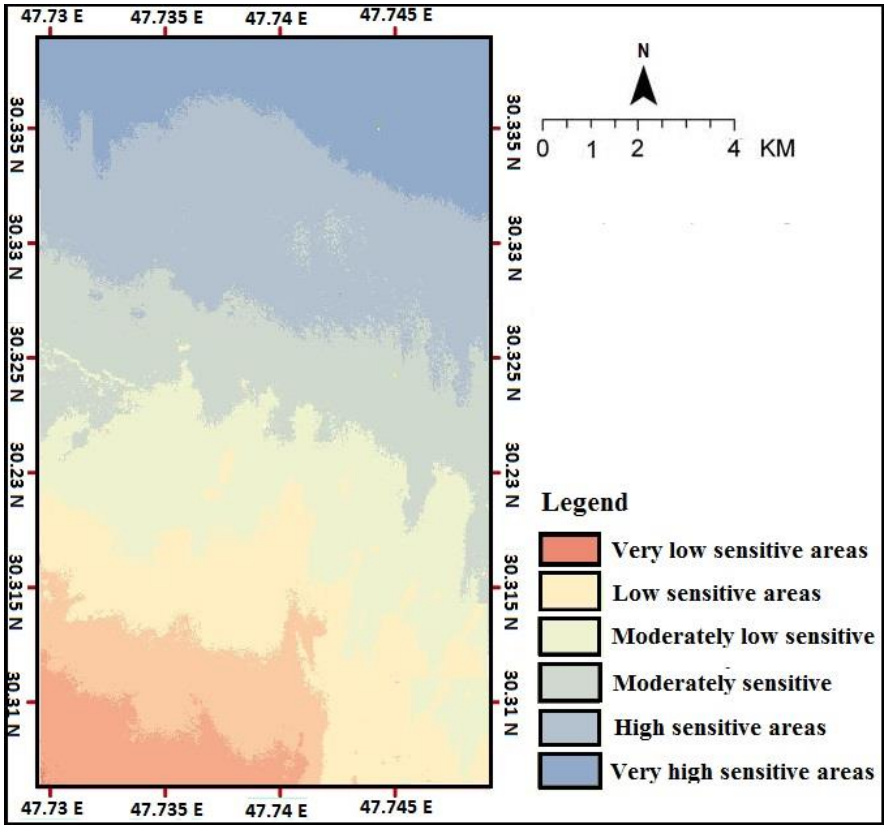

Fig. 5. Geostatistical distribution of salt affected area in the study area.

Factors causing soil salinity include inappropriate and excessive irrigation without adequate drainage system, irrigation water quality, rising saline water table, climate, rainfall history, local topography and soil composition and farming practices. Therefore, increasing soil salinity at the surface is most likely to vary according to the distribution of these different factors across the landscape. It was revealed that the spatial distribution was not highly influenced by the features considered except groundwater table. The results demonstrate that modeling and mapping spatial variation of soil salinity based on remote sensing data is a promising approach. Based on this view, to assess the distribution of saline soils, the water table map was overlaid with a map of salt affected soils. The rising water table brings salt from deep in the soil up to the surface, causing salt accumulation. The present results also suggested that a rising water table and salt accumulation at the surface combined with a high evaporation rate are likely factors that have resulted in the spatial variation in soil salinity of the area. This study shows how regression analysis, coupled with remote sensing images, could successfully predict and map spatial variation in soil salinity over an area vegetated. Thus, the information presented can help farmers, scientists and engineers to manage soil salinity problems affecting the ecosystem. Additionally, the simplicity of this approach, with its satisfactory accuracy, can contribute to soil salinity prediction and mapping at lower costs than conventional approaches.

Figure 6 and Table 6 shows the distribution of land degradation risk areas in study location, it is clear that the sensitive areas to land degradation in study area, where the soil quality, climatic quality and management quality are low; these areas represent 12.8 % of the study location area (i.e. 2.28 km^2). The areas of high to moderate sensitive for land degradation exhibit the rest of the parts of the study location as it represent 87.2 % of the total area (i.e. 15.51 km^2). The northern parts of the study location are characterized by a high risk for land degradation as they represent 61.9 % of the total area (i.e.11.01). The low risk for land degradation is due to the good vegetation cover and soil quality. The results of this study indicated that land degradation results from natural and anthropogenic factors. Overlay of land degradation processes layers interpreted from multi-temporal remotely sensed materials in a GIS, in conjunction with field investigation, revealed that the spatial extent of sandy desertified land in the area has drastically expanded during the fifteen-year study period (2000-2015).

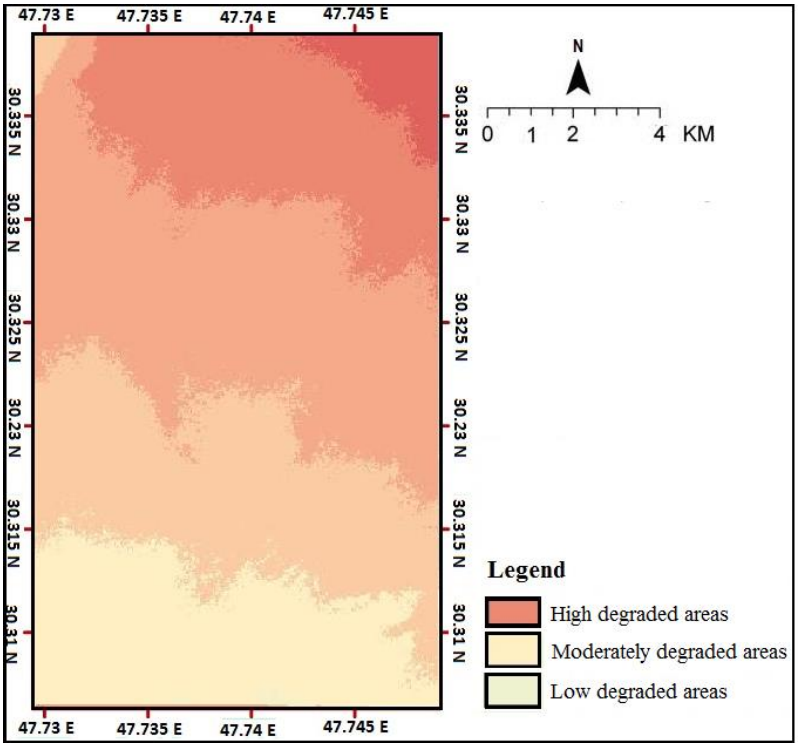

Fig. 6. Land degradation risk assessment in study area.

Land degradation processes in the study area was assessed through consideration of both natural (vegetative index, soil index, climatic index, drifting sand) and anthropogenic (Land use change) factors in the study. It was found that most of the study locations were highly land degradation. The overall sensitivity of land degradation change has worsened during the study period with degraded areas accounting for 61.9% of the total area in 2015. There is a clear trend in the spatial distribution of the land degradation direction within the study area, which goes from the Northwest toward the Southeast. The risk has risen considerably, on an average, by 40% for all western parts of study location between 2000 and

2015. In particular, the risk has increased considerably for those areas not previously considered highly vulnerable to degradation. Consequently, the disparity of land degradation hazard among the study locations has shrunk as all of them are at a higher risk in 2015 than ever before. The accentuation of land degradation is attributed to conflicts among human interest, limited land resource, and fragile ecosystems. Inappropriate human activities such as excessive exploitation of natural resource and mismanagement of land, to a certain extent, have contributed to the land destruction.

Table 6. The categories of land degradation and the proportion of each category

Class	Area (km^2)	%
Low land degradation areas	2.28	12.8
Moderately land degradation areas	4.50	25.3
High land degradation areas	11.01	61.9
Total	17.792	100

4. Conclusions

This study proposed a system depends on satellite images as the most important input data to the GIS, and it is ready to be imposed by other promoted required data for updating or any other environmental study in order to reduce the expense that is needed to construct other related study. It provides a tool more easily to manage the immediate attention with greater monitoring. Remote sensing and GIS based integration and spatial overlay soil salinity model using multivariate analysis results showed that most of the moderately saline soils are on saline water table depth. Intensive irrigation practices and excessive use of water and poor irrigation management can cause soil salinization. Areas where groundwater table lay above critical depth increased as a result of higher evaporation and this has contributed directly to the occurrence of moderate and slight salt accumulation in the area. The model has good predictability as it considers most of the factors, which contribute to soil salinization. Modeling and mapping spatial variation in soil salinity based on GIS analysis and remote sensing data are promising approaches, as it facilitates timely detection with a low-cost procedure and allow decision makers to decide on necessary actions, to be taken in the early stages to control soil salinity and to conserve agricultural lands and natural ecosystems.

Acknowledgments

The authors are grateful to the anonymous reviewers for their critical review and comments on drafts of this manuscript.

References

1. Allbed, A.; Kumar, L.; and Sinha P. (2014). Mapping and modelling spatial variation in soil salinity in the Al Hassa oasis based on remote sensing indicators and regression techniques. *Journal of Remote Sensing*, 6(2), 1137-1157.
2. Bilgili, A.V. (2013). Spatial assessment of soil salinity in the Harran plain using multiple kriging techniques. *Environmental Monitoring and Assessment*, 185(1), 777-795.

3. Dehni, A; and Lounis, M. (2012). Remote sensing techniques for salt affected soil mapping: application to the Oran region of Algeria. *Procedia Engineering*, 33,188-198.
4. Douaik, A.; Vanmeirvenne, M.; and Toth, T. (2005). Soil salinity mapping using spatiotemporal kriging Bayesian maximum entropy with interval soft data. *Geoderma*, 128(3-4), 234-248.
5. Metternicht, G.; and Zinck, J.A. (2003). Remote sensing of soil salinity: potentials and constraints. *Remote sensing of Environment*, 85(1),1-20.
6. Wu, J.; Vincent, B.; Yang, J.; Bouarfa, S.; and Vidal, A. (2008). Remote sensing monitoring of changes in soil salinity: a case study in Inner Mongolia, China. *Sensors*, 8(11), 7035-7049.
7. Wang, D.; Wilson, C.; and Shannon, M.C. (2002). Interpretation of salinity and irrigation effects on soybean canopy reflectance in visible and near-infrared spectrum domain. *International Journal of Remote Sensing*, 23(5), 811-824.
8. Khan, N.M.; Rastoskuev, V.V.; Sato, Y.; and Shiozawa, S. (2005). Assessment of hydrosaline land degradation by using a simple approach of remote sensing indicators. *Agricultural Water Management*, 77(1-3), 96-109.
9. Jabbar, M.T.; and Zhou, J. (2012). Assessment of soil salinity risk on the agricultural area in Basrah province, Iraq: using remote sensing and GIS techniques. *Journal of Earth Science*, 23(6), 881-891.
10. Tripathi, N.K.; Rai, B.K.; and Dwivedi, P. (1997). Spatial modeling of soil alkalinity in GIS environment using IRS data. *Proceedings of the 18th Asian Conference on Remote Sensing, Kualalampur*, 81-86.
11. Farifteh, J. (2007). Imaging spectroscopy of salt-affected soils: Model-based integrated method . *Utrecht University*, 143, (pp. 160).
12. Eldeiry, A.; and Garcia, L.A. (2008). Detecting soil salinity in alfalfa fields using spatial modeling and remote sensing. *Soil Science Society of America Journal*, 72(1), 201-211.
13. Royston, P.; and Sauerbrei, W. (2008). Multivariable model-building: a pragmatic approach to regression analysis based on fractional polynomials for modeling continuous variables, *John Wiley & Sons Chichester*, 777.
14. Awasthi, K.D.; Sitaula, B.K.; Singh, B.R.; and Bajacharaya, R.M. (2002). Land-use change in two Nepalese watersheds: GIS and geomorphometric analysis. *Land Degradation and Development*, 13(6), 495-513.
15. Velázquez, A.; Durán, E.; Ramírez, I.; Mas, J.F.; Bocco, G.; Ramírez, G.; and Palacio, J.L. (2003). Land use-cover change processes in highly biodiverse areas: the case of Oaxaca, Mexico. *Global Environmental Change*, 13(3), 175-184.
16. Al-Awadhi, J.M.; Omar, S.A.; and Misak, R.F. (2005). Land degradation indicators in Kuwait. *Land degradation and development*, 16(2), 163-176.
17. Gao, J.; Liu, Y.; and Chen, Y. (2006). Land cover changes during agrarian restructuring in northeast China. *Applied Geography*, 26(3-4), 312-322.
18. Liu, Y. ; Gao, J.; and Yang, Y. (2003). A Holistic approach towards assessment of Severity of land degradation along the great wall in northern Shaanxi province, China. *Environmental Monitoring and Assessment*, 82(2),187-202.